Journal of The Electrochemical Society

The Electrochemical Society
Advancing solid state & electrochemical science & technology

Electrochemistry of Protein Electron Transfer

To cite this article: Dmitry V. Matyushov 2022 *J. Electrochem. Soc.* **169** 067501

View the article online for updates and enhancements.

Investigate your battery materials under defined force!
The new PAT-Cell-Force, especially suitable for solid-state electrolytes!

EL-CELL®
electrochemical test equipment

- Battery test cell for force adjustment and measurement, 0 to 1500 Newton (0-5.9 MPa at 18mm electrode diameter)
- Additional monitoring of gas pressure and temperature

www.el-cell.com +49 (0) 40 79012 737 sales@el-cell.com

This content was downloaded from IP address 129.219.247.33 on 02/06/2022 at 16:12

Journal of The Electrochemical Society, 2022 **169** 067501
1945-7111/2022/169(6)/067501/6/$40.00 © 2022 The Electrochemical Society ("ECS"). Published on behalf of ECS by IOP Publishing Limited

Electrochemistry of Protein Electron Transfer

Dmitry V. Matyushov[z]

School of Molecular Sciences and Department of Physics, Arizona State University, Tempe, Arizona 85287-1504, United States of America

Protein fold and slow relaxation times impose constraints on configurations sampled by the protein. Incomplete sampling leads to the violation of fluctuation-dissipation relations underlying the traditional theories of electron transfer. The effective reorganization energy of electron transfer is strongly reduced thus leading to lower barriers and faster rates (catalytic effect). Electrochemical kinetic measurements support low activation barriers for protein electron transfer. The distance dependence of the rate constant displays a crossover from a plateau at short distances to a long-distance exponential decay. The transition between these two regimes is controlled by the protein dynamics.
© 2022 The Electrochemical Society ("ECS"). Published on behalf of ECS by IOP Publishing Limited. [DOI: 10.1149/1945-7111/ac60f1]

Manuscript submitted December 27, 2021; revised manuscript received March 3, 2022. Published June 1, 2022. *This paper is part of the JES Focus Issue on Biosensors and Nanoscale Measurements: In Honor of Nongjian Tao and Stuart Lindsay.*

Transport of electrons is an essential part of the energetic machinery of life. This process is accompanied by the transfer of positively charged protons in the direction opposite to electrons, leading to the protonmotive force supplying energy to biology.[1]

This perspective article is concerned with individual electron hops between redox cofactors in the electron transport chain. Such transitions have been traditionally described by the Marcus theory developed for electron-transfer reactions in polar liquid solvents.[2] Because of its general scope addressing the effect of Gaussian medium fluctuations on electron tunneling between localized electronic states, the theory has enjoyed wide-spread applications to complex media for which it was not originally intended, including long-distance electron transfer in redox-active proteins.[3]

There are a number of unique properties of proteins that set them apart from simple polar liquids.[4] These distinctions include a strong coupling between elastic motions and electrostatic interactions of the protein-water interface and constrained and frustrated character of the protein interior[5] and its hydration shell.[6] The active sites of enzymatic catalysis and redox reactions are immersed in a heterogeneous environment with no simple rules for the screening of polar interactions and many time scales of molecular motions. Yet this complex spectrum of fluctuations projects itself on a few generic parameters entering the activation barrier of electron transfer. Like in the standard Marcus formulation, the description of the activation barrier is still reduced to two parameters, the reorganization energy and the reaction free energy, but the former, the reorganization energy, becomes an effective gauge of the work required to polarize the system to achieve the tunneling configuration for electron transfer.

As we discuss here, the spatial, dynamic, and statistical complexity of the protein-water thermal bath requires[7] lifting the relation imposed on the parameters of the Marcus theory by the fluctuation-dissipation theorem (FDT).[8] This relation is the equality between the reorganization energy derived from the first moments (the Stokes shift) and the reorganization energy from the variance of the reaction coordinate (spectral width for charge-transfer transitions). Instead of being equal, these two distinct parameters are combined in an effective reaction reorganization energy, which is the only reorganization parameter accessible by kinetic experiments. This effective reorganization energy is strongly reduced for protein electron transfer compared to direct calculations based on the Marcus theory thus leading to lower activation barriers and faster reactions.

Standard Theory

The rate constant of electron transfer k_{ET} in the Marcus-Levich theory[2,9] is a product of the tunneling factor $2\pi V^2/\hbar$ from the golden-rule expression for electronic transitions and the statistical-mechanical probability $P(X=0)$ of reaching the resonance condition $X=0$ for electron tunneling

$$k_{ET} = (2\pi V^2/\hbar) \times P(X=0) \quad [1]$$

Here, V is the electronic coupling between the localized states and $\hbar$ is Planck's constant. The probability density $P(X)$ describes the statistical distribution of the energy difference[10] $X = E_A - E_D$ between the electronic states of the acceptor, E_A, and the donor, E_D. The tunneling configuration is reached when the energy gap is zero, $X=0$.

The standard theory is formulated for the transferring electron interacting with many particles in the medium. By central limit theorem, $P(X)$ is a Gaussian function defined by two statistical moments: the average, $\langle X\rangle$, and the variance, $\sigma_X^2 = \langle(\delta X)^2\rangle$, $\delta X = X - \langle X\rangle$

$$P(X) \propto \exp\left[-\frac{(X-\langle X\rangle)^2}{\sigma_X^2}\right] \quad [2]$$

The free energy of electron transfer is given as the logarithm of the probability function

$$F(X) = -k_B T \ln[P(X)] \quad [3]$$

The free energy function is a parabola with the minimum at $\langle X\rangle$.

There are two electronic states involved in electron transfer and one needs to define two parabolas with minima $\langle X\rangle_i$, where $i=1$ and $i=2$ correspond to the reactant and product configurations, respectively. This is the Marcus picture of crossing parabolas. The physical interpretation of two different values $\langle X\rangle_i$ is that the electron localized at the donor or the acceptor polarizes the medium and the shift $\Delta X = |\langle X\rangle_2 - \langle X\rangle_1|$ reflects the change in the interaction energy of the transferring electron with the sluggish (nuclear) part of the medium polarization.

One additional assumption, on the top of the Gaussian statistics of X, enters the standard description. This is the assumption of the Gibbsian statistics of the medium configurations, which postulates that the system can sample the entire manifold of M degrees of freedom $q_1,\ldots,q_M$ coupled to the electron. Figure 1 is a cartoon illustration of this physical picture for only two coordinates, q_1 and q_2. Importantly, the medium is not hindered to establish full equilibrium with the altering charge distribution, as is schematically indicated by the medium dipoles oriented along the electric field produced by the transferring electron. This standard picture does not fully apply to the heterogeneous and highly frustrated protein-water thermal bath, with significant consequences for the activated kinetics.

The result of applying the Gibbsian statistics to the medium coordinates is expressed by the FDT[8] connecting the shift in the

[z]E-mail: dmitrym@asu.edu

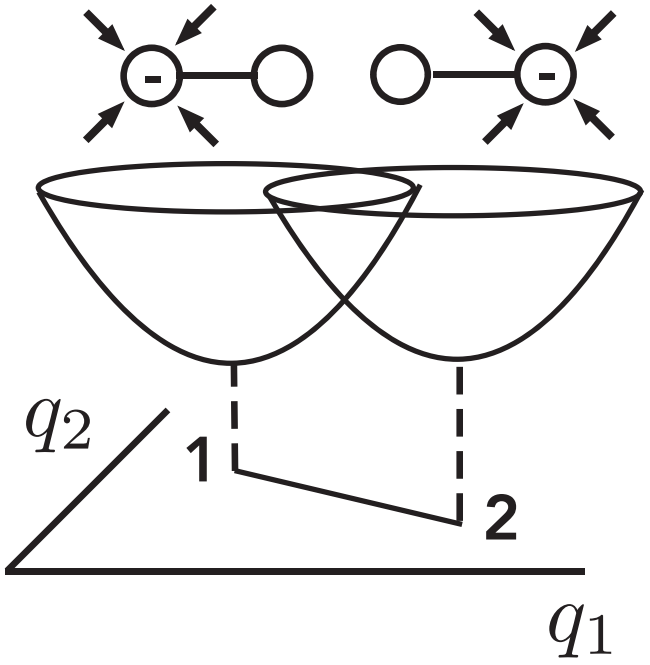

Figure 1. Crossing parabolas plotted against the configuration space of medium coordinates q_1 and q_2 coupled to the transferring electron. The polarization of the medium, schematically shown by dipole moments, is in full equilibrium with both states of the electron.

average energy gap ΔX to the Gaussian variance σ_X^2 expressed in terms of the Marcus reorganization energy λ: $\sigma_X^2 = 2k_B T\lambda$. This relation is conveniently represented by introducing the Stokes-shift reorganization energy $2\lambda^{St} = \Delta X$. The FDT establishes[7] a single reorganization energy to specify the statistics of X

$$\lambda^{St} = \lambda \qquad [4]$$

The celebrated Marcus equation for the activation barrier of electron transfer[2] is a direct consequence of imposing this relation

$$\Delta G^{\dagger} = \frac{(\lambda + \Delta G_0)^2}{4\lambda} \qquad [5]$$

Here, ΔG_0 is the standard reaction free energy.

Protein Electron Transfer

The protein thermal bath presents an environment distinctly different from a simple polar liquid considered in the standard Marcus formulation. The dipoles of the medium are constrained by the protein fold and cannot freely rotate to adjust to the changing field of the active site.[11] Figure 2 illustrates this by showing protein helices. The dipoles of amino acids ($\simeq$4.5–5 D per residue[12]) add up to a large total dipole of the helix, which is approximately equal to $(0.5 - 0.7)e \times L_{helix}$,[13] where L_{helix} is the helix length and e is the elementary charge. However, this large dipole is mostly fixed by the protein fold and cannot rotate in response to the field of the electron, in contrast to the situation depicted in Fig. 1.

Because of the protein fold and tight packing,[14] the configuration space of the medium is constrained and frustrated by both geometric and energetic restrictions imposed on the medium displacements. To exemplify this note, large dipoles of protein helices, despite their large magnitudes,[12,13] cannot produce significant dipolar fluctuations, with the overall low dielectric constant specific to the protein interior. One might think that the dipole moments of the protein segments can shift in response to altering charge (as is illustrated by deformed protein helices in Fig. 2), but experimental evidence shows little structural rearrangement in response to charge transfer. In

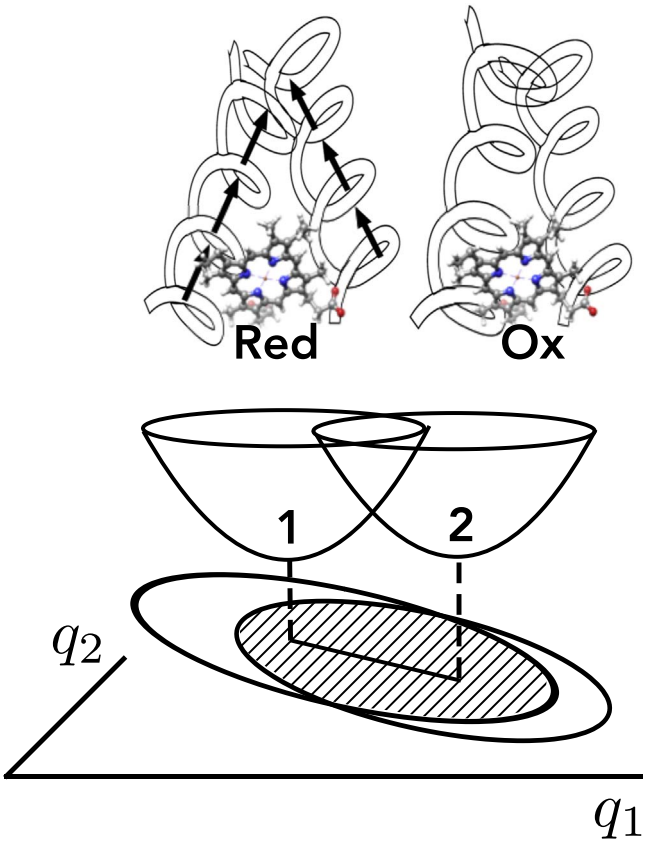

Figure 2. Constrained configuration space of the thermal bath for protein electron transfer. The dipoles of the protein medium are constrained by the protein fold and do not reorient in response to the altering field of the active site. The configuration space available to both states is the overlap (shaded area) of restricted configuration spaces of each oxidation state.

contrast to the picture shown in Fig. 1, altering charge of the active site cannot compete with much stronger geometrical constraints and other interactions regulating an essentially unperturbed protein structure.

The geometry of the protein can in principle alter when triggered by changing oxidation state, but there is no guarantee that a new medium polarization will be proportional to the field of the active site, as is the case for polar liquids. One can think of such structural changes more in terms of transitions between local minima on the energy landscape[5,15] than a continuous deformation of an effective spring representing the medium, which is the mechanistic model behind two shifted parabolas in Fig. 1. A small localized change in the structure is not equal to a global shift of equilibria of many microscopic oscillators representing the medium.

Hydration water can be more flexible in response to charge transfer, but this part of the medium is also constrained by strong interfacial fields of the protein ionized residues and frustrated by competing orientations of water clusters oriented by the mosaic of negative and positive residues at the surface of a typical folded protein.[6] The properties of hydration water are significantly altered from those of the bulk,[16] including a significant reduction of water's polar response.[17]

The protein fold and its frustrated hydration shell impose severe restrictions on the configurations affecting the energy states of the electron localized at an active site. Importantly, the configuration space available to both oxidation states comes as an overlap of restricted configuration manifolds of each state and is therefore even further restricted (shaded area in Fig. 2). Imposing constraints is equivalent of moving the system to a new equilibrated state with a lower entropy[18] (sometimes specified as a metastable state). The

spectrum of spontaneous fluctuations in such a nonequilibrium state must be altered compared to the the fully equilibrated state in which constraints have been lifted. For a functioning enzyme, one can argue that the entire set of configurations corresponding to the protein unfolded state is eliminated from the configuration space, but there are many additional constraints including those dynamic in character (see below).

The direct consequence of restrictions on the medium response imposed by the protein scaffold is that the standard FDT link between the first an second statistical moments of the reaction coordinate X is broken for protein electron transfer.[7,19] This is reflected by two distinct reorganization energies related by the following inequality

$$\lambda^{\mathrm{St}} < \lambda \qquad [6]$$

in place of the equality between them in the Marcus theory (Eq. 4). This inequality implies that even though a sufficient shift of the equilibrium configuration is not allowed by the protein fold, electrostatic fluctuations around corresponding equilibria are still mostly allowed. In fact, electrostatic fluctuations at protein active sites are even more intense than typically found for molecular solutes in polar liquids.[20] They are driven by the coupling between elastic modulations of the global protein shape and hydration water arrested in the interface by strong electric fields of the ionized residues. The hydration water follows adiabatically fluctuations of the protein shape, thus enhancing the electrostatic noise at the active site. Such electroelastic interfacial fluctuations (analogous to the piezoelectric effect in solid materials) lead to large values of σ_X^2 reported by simulations of solvated proteins and corresponding large values of λ exceeding λ^{St} by a factor of 2–5.[19]

The mechanistic consequence of a strong electrostatic noise produced by the protein-water interface is that the Marcus parabolas are flattened and their crossing point is achieved at a lower activation barrier. It is expressed mathematically by replacing the Marcus reorganization energy in the expression for the activation barrier (Eq. 5) with the effective (reaction) reorganization energy

$$\lambda^r = \frac{(\lambda^{\mathrm{St}})^2}{\lambda} \qquad [7]$$

Because of the inequality in Eq. 6, this effective reorganization energy is lowered compared to the standard Marcus prediction. Lower activation barriers and faster reactions follow as a result.

Nonergodic Protein Fluctuations

Constraints imposed by the protein fold on accessible protein configurations convert the Gibbsian ensemble for the thermal bath to a restricted ensemble in which some of the system configurations are never reached. Such constraints can be both static and dynamic. The dynamic constraints imply that some movements of the system are too sluggish to occur on the reaction time scale, and they simply never happen. In other words, a part of the configuration space that is accessible in principle is dynamically frozen on the reaction time. This situation is known as glassy dynamics,[5,15] which seem to apply to biology on different length scales, including the elastic response of the entire cell.[21]

The phenomenology of dynamic freezing of configuration space is particularly significant for fast reactions of primary charge transfer in photosynthesis.[22] Primary charge separation follows absorption of a photon by the primary pair in bacterial photosynthesis and by P680 pigment in photosystem II.[1,22] It occurs on a very short reaction time of $(k_{\mathrm{ET}})^{-1} < 10$ ps. Much of protein dynamics are dynamically frozen on that time scale and the reorganization energy has to be calculated for a specific time window. This is achieved by turning to the spectral density of the energy gap fluctuations, which accounts for the relative weight of each frequency in the fluctuation spectrum to the overall Gaussian variance σ_X^2.

The relaxation processes in the heterogeneous protein-water system are dissipative and in most cases are better described by Langevin overdamped dynamics than by oscillatory motions often explored by the normal-mode analysis. The analysis is thus cast in terms of the relaxation times of the properties of interest, which is the reaction coordinate $X(t)$ for for electron-transfer reactions. The Stokes-shift relaxation function is defined as the time autocorrelation function of $X(t)$: $C_X(t) = \langle \delta X(t) \delta X(0) \rangle$. The loss (or power) spectrum is defined by the loss function $\chi_X{}''(\omega) \propto \omega \tilde{C}(\omega)$ in terms of the time Fourier transform $\tilde{C}_X(\omega)$ of the correlation function. The representation in terms of the loss spectrum is convenient since each peak of $\chi_X{}''(\omega_{\max})$ specifies a relaxation process with the relaxation time given by the reciprocal frequency of the maximum $\omega_{\max}^{-1}$. The peak height specifies the faction of the energy dissipated by a specific relaxation process (loss) to the heat bath. If the entire range of frequencies $0 \leqslant \omega < \infty$ is allowed, the loss spectrum integrates to the thermodynamic reorganization energy $\lambda = \sigma_X^2/(2k_{\mathrm{B}}T)$. Alternatively, a low-frequency cutoff, given by the electron-transfer rate $k = k_{\mathrm{ET}}$, is applied to the frequency integral to define the nonergodic reorganization energy[23] when dynamic freezing applies

$$\lambda(k) = \int_k^\infty (d\omega/\omega)\chi''_X(\omega) \qquad [8]$$

In this equation, the thermodynamic limit $\lambda = \lambda(0)$ follows by putting $k = 0$. This limit corresponds to the standard assumption of equilibrium thermodynamics that the observation window k^{-1} is infinitely long, thus allowing the system in contact with a thermal bath to visit all possible configurations (ergodicity). Ergodicity is an idealization and is never reached in practice. What is practically required for reaching the thermodynamic limit[24] is the condition $k\tau_{\min} \ll 1$ for the lowest relaxation time $\tau_{\min}$ in the loss spectrum. This requirement ensures that all processes affecting the reaction coordinate have equilibrated on the reaction time k^{-1}.

The frequency cutoff severely reduces the reorganization energy for primary charge separation from its thermodynamic value $\lambda \simeq 2.36$ eV to a much lower nonergodic value $\lambda(k_{\mathrm{ET}}) \simeq 0.36$ eV[20,25] produced by fast, ballistic local vibrations of molecular groups always present in condensed materials. Therefore, this value sets the lower boundary for the variance reorganization energy. If the thermodynamic reorganization energy applied to primary charge separation, bacterial photosynthesis would not be possible energetically since the energy dissipated to the heat bath would exceed the energy of the light photon. Nevertheless, even lower reaction reorganization energy λ^r can be achieved for electron transfer on the 1–100 ns reaction time. This is because this time window allows electroelastic fluctuations arising from elastic motions shifting surface ionized residues that strongly enhance the electrostatic noise at the active site leading to a large λ. At the same time, constraints imposed by the protein fold on geometry changes lead to a small λ^{St} in Eq. 7.

Electron-transfer hops on the time scale of 1–100 ns are still nonergodic in respect to slow conformational and segmental motions of the protein occurring on much longer time scales from milliseconds up to 10^2 s.[26–28] These slow modes are responsible for the dynamic heterogeneity,[29] i.e., a distribution of enzymatic reaction rates observed by single-molecule experiments.[30–32] Single-molecule studies have suggested that the active space of a reacting enzyme is a small sub-ensemble of "hot" states, while the majority of configurations remain inactive.[33] The shaded area in Fig. 2 pictures such a "hot" subspace in the configuration space of a redox active protein.

The arguments presented for the reorganization energy (a free energy in the thermodynamic limit) should equally apply to the reaction free energy ΔG_0. In linear solvation theories, λ and ΔG_0 follow from the same susceptibility functions and are physically and computationally related. The situation is more complex in nonergodic systems since ΔG_0, in terms of Eq. 8, is specified by the time window that the system spends in the initial and final reaction states,

instead of the rate constant k for the reorganization energy. This situation is common for glassy systems, which depend on the route of "preparation", e.g., on the rate of quenching of a bulk glass-former.[34] For the electrochemical experiment considered next, we assume that the electrode potential has a sufficient time to reach its equilibrium value corresponding to zero electrode overpotential. The problem of nonergodic reaction free energy does not appear in this setup and will not be considered.

Protein Electrochemistry

Electron-transfer reorganization energies are often extracted from kinetic studies in which both the donor and acceptor belong to the same protein molecule, such as in Ru-modified metalloproteins when the electron is injected to the active site from the photoexcited $Ru(bpy)_2$ complex.[3] Kinetics of electron transfer can be alternatively studied by electrochemistry, when electrons are exchanged between the metal electrode and active sites in half redox reactions. These two approaches have produced distinct sets of data. While solution studies report $\lambda^r \simeq 0.7$–0.8 eV,[3] a number of electrochemical measurements[35–40] and electrochemical scanning tunneling microscopy[41,42] have produced significantly lower, $\simeq 0.2 - 0.6$ eV, reorganization energies of half reactions. The results of solution experiments are affected by a redox group exposed to water, which often dominates in the overall reorganization energy. Given this complication, redox half reactions potentially provide a more reliable access to the reorganization energy of the active site.

Nonergodic protein electron transfer discussed above is fully applicable to protein electrochemistry. The mechanistic distinction of the electrochemical setup requires accounting for a continuum of electronic metal states. The summation of Golden Rule transitions to filled electronic state of the metal leads[43,44] to the following cathodic rate constant

$$k_c(\eta) = \frac{\langle\Delta\rangle}{\hbar}\,\mathrm{erfc}\left[\frac{\lambda^r + e\eta}{\sqrt{4\lambda^r k_B T}}\right] \qquad [9]$$

where $\mathrm{erfc}(x)$ is the complimentary error function, η is the electrode overpotential, and Δ is the electronic coupling between the protein and the electrode.[45] The reason it enters the equation for the rate as an average value $\langle\Delta\rangle$ is because proteins are loosely attached to the self-assembled monolayer (SAM).[43] The exponential decay $\Delta \propto \exp[-\gamma R]$ of the tunneling probability with the distance to the electrode R is modulated by protein motions at the SAM surface. If the protein is restrained to the SAM by a harmonic potential, one obtains[46]

$$\langle\Delta\rangle = \Delta_e e^{\gamma^2\langle\delta R^2\rangle/2} \qquad [10]$$

where Δ_e refers to the equilibrium distance to the electrode and $\langle\delta R^2\rangle$ is the variance of the protein-electrode distance.

The modulation of the tunneling distance by protein translations and conformational motions is distinct from fluctuations of super-exchange electronic coupling in protein electron transfer.[47] In this mechanism, fluctuations of electronic states in the medium separating the donor and acceptor lead to fluctuations of the tunneling probability and, in cases of electronic degeneracy, to "flickering resonances".[48]

Translational motions of the protein relative to the electrode modify not only the electron-protein tunneling probability, but also the preexponential factor of the rate. Theories of solvent-controlled electron transfer[49,50] show that the rate preexponent is affected by the competition between the rate of tunneling $\Delta_e/\hbar$ and the rate of the solvent Stokes-shift dynamics τ_x^{-1}, where τ_x is the relaxation time of the Stokes-shift time correlation function $\propto \langle\delta X(t)\delta X(0)\rangle$. Medium dynamics modify the preexponential factor of the cathodic rate to the following equation

$$k_c^s(\eta) = (1 + g)^{-1} k_c(\eta) \qquad [11]$$

with the tunneling rate constant $k_c(\eta)$ given by Eq. 9. The standard theories[49] of electron transfer controlled by solvent dynamics

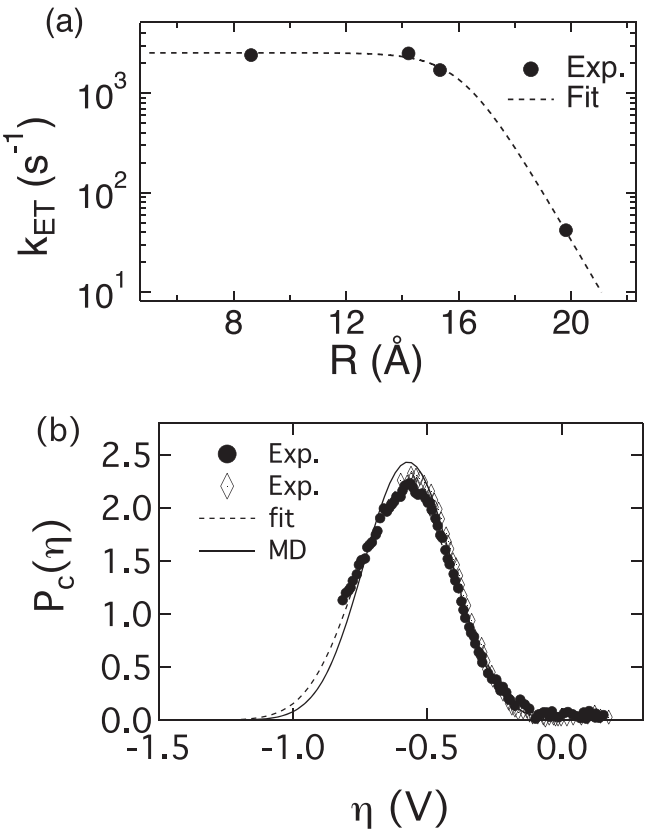

Figure 3. (a) Experimental (Exp.) data for reduction of Cyt-c[52] on PyC_n/C_{n-1} SAM ($n = 6$, 11, 12, 16) coating the gold electrode (points), $T = 298$ K. The dashed line is the fit to Eq. 11. (b) Normalized probability density $P_c(\eta)$ (Eq. 15) obtained from experiments with tuna (filled circles[54]) and horse (diamonds[35]) Cyt-c and from MD simulations (solid line). The dashed line is the Gaussian fit through the filled circles; no fitting parameters are applied to the MD results.

produce[46]

$$g \simeq 8\tau_x k_B T \Delta_e/(\hbar\lambda^r) \qquad [12]$$

A testable theory prediction is leveling off of the reaction rate constant as a function of the protein-electrode equilibrium distance R_e when the electronic coupling Δ_e becomes sufficiently high to allow $g > 1$ in Eqs. 11 and 12. This is indeed observed experimentally (Fig. 3), but the time $\tau_{\mathrm{eff}} \simeq 188$ ns required to fit the experimental data[51,52] for cytochrome c (Cyt-c) to Eqs. 11 and 12 significantly exceeds $\tau_x \simeq 0.3$–0.9 ns ($T = 280$–360 K) from molecular dynamics (MD) simulations.[53]

The difficulty with fitting the experimental data is resolved by recognizing that diffusional dynamics of the protein at the SAM surface leads to yet another characteristic time scale entering the rate pre-exponential factor. If the diffusion constant of translational diffusion is D, the tunneling probability is modulated with the relaxation time

$$\tau_\gamma = (\gamma^2 D)^{-1} \qquad [13]$$

It enters the parameter g in Eq. 11

$$g = \exp\left[\frac{3}{2}\gamma^2\langle\delta R^2\rangle\right]\frac{\Delta_e\tau_\gamma}{\hbar} \qquad [14]$$

when translational dynamics of the protein dominate over the Stokes-shift dynamics. A complete solution of the problem switches g to the standard result in Eq. 12 when the protein is fixed at a specific distance from the electrode and the Stokes-shift dynamics dominate.[46]

Equations 11 and 14 resolve the problem of the relaxation time τ_{eff} being inconsistent with τ_x and reconcile theory with experiment.[40] Following a plateau at short distances, the rate constant decays exponentially with increasing distance as predicted by Eq. 9. In this regime, the derivative of the rate constant over the overpotential, $dk_c/d\eta$, is proportional to the "density of states" of the oxidized energy level in the medium

$$P_c(\eta) \propto \exp\left[-\frac{(\lambda^r + e\eta)^2}{4\lambda^r k_B T}\right] \qquad [15]$$

The distribution function $P_c(\eta)$ is directly accessible from cyclic voltamemtry upon correction for mass transport.[55] The corresponding experimental data for Cyt-c[35,54] are shown by points in Fig. 3b.

The experimental results in Fig. 3b are compared to direct calculations from MD simulations (solid line). The agreement is very good, leading to the overall solvent reorganization energy of $\lambda^r \simeq 0.57$ eV. Noteworthy is that full sampling of λ was achieved with ~300 ns simulations, which is monitored by finding $\lambda^{St} \simeq \lambda \simeq 1.3 - 1.6$ eV for the standard model of the active site represented by point atomic charges. This value is much higher than experiment, and the agreement shown in Fig. 3b is achieved by accounting for the polarizability of the heme cofactor. The heme polarizability is highly anisotropic and is highest in the heme plane. The heme is strategically positioned in the protein pocket such that its polarizability anisotropy matches anisotropy of electric field fluctuations, which are also strongest in the heme plane. The combination of these two factors lifts λ to $\simeq$2.85 eV, thus reducing λ^r (Eq. 7) to the value consistent with kinetic measurements.

Simulations of Cyt-c have indicated that nonergodic sampling allowing the catalytic effect might not always be accomplished, particularly for small globular proteins. Indeed, the strongest separations between two reorganization energies in Eq. 6 have been found in simulations of complex membrane-bound protein systems (reaction centers,[20] bc_1 complexes,[56,57] and complex I[58]). Small proteins might require alternative mechanisms for lowering the activation barrier. For small globular proteins with $\lambda^{St} \simeq \lambda$ for the overall protein-water reorganization, the protein component alone still shows a strong separation of the Stokes-shift and variance reorganization energies (Eq. 6).[59] Therefore, partial dehydration of the protein in the process of binding to interfaces and/or to larger protein complexes might be a physical mechanism leading to the separation of reorganization energies on Eq. 6. Water, as a fast and adjustable component of the protein-water thermal bath, can provide structural changes of the medium that are not anticipated in traditional theories of electron transfer in polar liquids.[2] The force constant (or the parabolas curvature) of an effective spring representing the medium in these theories is not altered upon charge transfer. The possibility of charge-induced partial hydration of the active site alters this paradigm. Changes in the active site hydration upon charge transfer were found in simulations of bacterial photosynthesis,[60] in charge-transfer chain of Complex I of respiratory energy chains,[58] and for a small redox protein ferredoxin[61] which, like Cyt-c, participates in shuttling electrons between large protein complexes. Such structural changes lead to different force constants of the effective medium spring in two charge-transfer states and cannot be described by the picture of crossing parabolas.[62]

Conclusions

Kinetic electrochemical measurements of protein electron transfer have demonstrated low values for the protein reorganization energy $\lambda^r \simeq 0.2$–0.6 eV. Specific physical mechanisms have been recognized that lead to these observations through the separation between the Stokes and variance reorganization energies (Eq. 6). Despite different mechanisms involved, natural selection seems to favor such a separation, violating the FDT, to allow low barriers and fast reactions.

Modulation of the tunneling probability by protein motions leads to the appearance of a new time scale (Eq. 13) affecting the pre-exponential factor of the rate constant. The rate constant is distance-independent and friction-controlled (Fig. 3a) at small distances, followed by an exponential decay at longer distances. This is a general phenomenology that must apply broadly. For instance, weak binding is realized in biological energy chains, where small redox-active proteins shuttle electrons to larger membrane-bound protein complexes. In addition, conformational flexibility of a large protein complex should modulate distances between protein cofactors in intraprotein electron transport. The principal result of both theory and experiment is that charge transfer is friction-controlled at $R_e \leqslant 15$ Å. Within this distance, which essentially specifies the range of activated biological electron transfer,[63] the charge hopping rate remains nearly constant (Fig. 3a). This picture is in sharp contrast with the commonly adopted view that the rate of electron transfer decays exponentially with distance for all cofactors in the protein matrix.[3]

The notion of incomplete sampling of the configuration space and of the nonergodic activation barrier for electron transfer provides a mechanism for the catalytic effect by redox proteins and, potentially, for charge conductivity by proteins.[64] A number of challenges to understanding the fundamental mechanisms of charge transport in biological energy chains still remains. The role of electrowetting, i.e., changes in hydration of protein active sites, is far from fully appreciated. This mechanism leads to non-parabolic free energy surfaces of electron transfer and requires both mechanistic studies and new theoretical models. The problem of vectorial, unidirectional electron transfer in biological energy chains has not been studied theoretically. The current paradigm requires the downhill free energy profile for the unidirectional charge transport. Can this picture be amended by changes in the protein dynamics along the charge path to allow nonergodic mechanisms to drive the reaction in a specific direction? These are still questions which have not been consistently posed or formulated in terms of mathematical and computational algorithms.

Acknowledgments

This research was supported by the National Science Foundation (CHE-2154465) and by the Army Research Office (ARO-W911NF2010320).

ORCID

Dmitry V. Matyushov https://orcid.org/0000-0002-9352-764X

References

1. D. G. Nicholls and S. J. Ferguson, *Bioenergetics* (Academic, Amsterdam) 4 (2013).
2. R. A. Marcus and N. Sutin, *Biochim. Biophys. Acta*, **811**, 265 (1985).
3. H. B. Gray and J. R. Winkler, *Proc. Natl. Acad. Sci.*, **102**, 3534 (2005).
4. A. Cooper, *Prog. Biophys. Molec. Biol.*, **44**, 181 (1984).
5. H. Frauenfelder, G. Chen, J. Berendzen, P. W. Fenimore, H. Jansson, B. H. McMahon, I. R. Stroe, J. Swenson, and R. D. Young, *Proc. Natl. Acad. Sci. USA*, **106**, 5129 (2009).
6. D. R. Martin and D. V. Matyushov, *J. Phys. Chem. Lett.*, **6**, 407 (2015).
7. D. V. Matyushov, *J. Chem. Phys.*, **139**, 025102 (2013).
8. R. Kubo, *Rep. Prog. Phys.*, **29**, 255 (1966).
9. V. G. Levich, *in Advances in Electrochemistry and Electrochemical Engineering*, ed. P. Delahay (Interscience, New York, NY) 1 (1965).
10. A. Warshel, *J. Phys. Chem.*, **86**, 2218 (1982).
11. L. I. Krishtalik, *Phys.-Usp.*, **55**, 1192 (2012).
12. Y.-D. Wu and Y.-L. Zhao, *J. Am. Chem. Soc.*, **123**, 5313 (2001).
13. W. G. J. Hol, *Adv. Biophys.*, **19**, 133 (1985).
14. J. C. Gaines, A. H. Clark, L. Regan, and C. S. O'Hern, *J. Phys.: Condens. Matter J. Phys.: Condens. Matter*, **29**, 293001 (2017).
15. J. Brujić, R. I. H. Z. K. A. Walther, and J. M. Fernandez, *Nat. Phys.*, **2**, 282 (2006).
16. M.-C. Bellissent-Funel, A. Hassanali, M. Havenith, R. Henchman, P. Pohl, F. Sterpone, D. van der Spoel, Y. Xu, and A. E. García, *Chem. Rev.*, **116**, 7673 (2016).
17. D. V. Matyushov, *J. Phys. Chem. B*, **125**, 8282 (2021).
18. H. Reiss, *Methods of Thermodynamics* (Dover Publications, Inc., Mineola, N. Y.) (1996).
19. D. V. Matyushov, *J. Phys.: Condens. Matter J. Phys.: Condens. Matter*, **27**, 473001 (2015).

20. D. N. LeBard and D. V. Matyushov, *Phys. Chem. Chem. Phys.*, **12**, 15335 (2010).
21. X. Trepat, L. Deng, S. S. An, D. Navajas, D. J. Tschumperlin, W. T. Gerthoffer, J. P. Butler, and J. J. Fredberg, *Nature*, **447**, 592 (2007).
22. R. E. Blankenship, *Molecular Mechanisms of Photosynthesis* (Blackwell Science, Williston, VT) (2003).
23. D. V. Matyushov, *J. Chem. Phys.*, **122**, 084507 (2005).
24. R. P. Feynman, *Statistical Mechanics* (Westview Press, Boulder, CO) (1998).
25. H. Wang, S. Lin, J. P. Allen, J. C. Williams, S. Blankert, C. Laser, and N. W. Woodbury, *Science*, **316**, 747 (2007).
26. L. Edman, Z. Földes-Papp, S. Wennmalm, and R. Rigler, *Chem. Phys.*, **247**, 11 (1999).
27. B. P. English, W. Min, A. M. van Qijen, K. T. Lee, G. Luo, H. Sun, B. J. Cherayil, S. C. Kou, and X. S. Xie, *Nat. Chem. Biol.*, **2**, 87 (2006).
28. L. Iversen et al., *Science*, **345**, 50 (2014).
29. X. S. Xie, *Science*, **342**, 1457 (2013).
30. H. Yang, G. Luo, P. Karnchanaphanurach, T.-M. Louie, I. Rech, S. Cova, L. Xun, and X. S. Xie, *Science*, **302**, 262 (2003).
31. A. Gupta, T. J. Aartsma, and G. W. Canters, *J. Am. Chem. Soc.*, **136**, 2707 (2014).
32. B. Pradhan, C. Engelhard, S. V. Mulken, X. Miao, G. W. Canters, and M. Orrit, *Chem. Sci.*, **11**, 763 (2019).
33. H. Engelkamp, N. S. Hatzakis, J. Hofkens, F. C. De Schryver, R. J. M. Nolte, and A. E. Rowan, *Chem. Commun.*, **327**, 935 (2006).
34. P. G. Debenedetti, *Metastable Liquids: Concepts and Principles* (Princeton University Press, Princeton, NJ) (1996).
35. J. Cheng, S. Terrettaz, J. I. Blankman, C. J. Miller, B. Dangi, and R. D. Guiles, *Israel J. Chem.*, **37**, 259 (1997).
36. J. J. Wei, H. Liu, K. Niki, E. Margoliash, and D. H. Waldeck, *J. Phys. Chem. B*, **108**, 16912 (2004).
37. Y. Guo, J. Zhao, X. Yin, X. Gao, and Y. Tian, *J. Phys. Chem. C*, **112**, 6013 (2008).
38. D. E. Khoshtariya, T. D. Dolidze, M. Shushanyan, K. L. Davis, D. H. Waldeck, and R. van Eldik, *Proc. Natl. Acad. Sci. USA*, **107**, 2757 (2010).
39. S. Monari et al., *J. Am. Chem. Soc.*, **134**, 11848 (2012).
40. U. A. Zitare, J. Szuster, M. C. Santalla, M. N. Morgada, A. J. Vila, and D. H. Murgida, *Electrochim. Acta*, **342**, 136095 (2020).
41. Q. Chi, O. Farver, and J. Ulstrup, *Proc. Natl. Acad. Sci. USA*, **102**, 16203 (2005).
42. A. Alessandrini, S. Corni, and P. Facci, *Phys. Chem. Chem. Phys.*, **8**, 4383 (2006).
43. C. E. D. Chidsey, *Science*, **251**, 919 (1991).
44. N. S. Hush, *J. Electroanal. Chem.*, **470**, 170 (1999).
45. W. Schmickler and E. Santos, *Interfacial Electrochemistry* (Springer, Berlin) 2nd ed. (2010).
46. D. V. Matyushov, *J. Phys. Chem. B*, **123**, 7290 (2019).
47. S. S. Skourtis, D. H. Waldeck, and D. N. Beratan, *Annu. Rev. Phys. Chem.*, **61**, 461 (2010).
48. Y. Zhang, C. Liu, A. Balaeff, S. S. Skourtis, and D. N. Beratan, *Proc. Natl. Acad. Sci. USA*, **111**, 10049 (2014).
49. H. Sumi and R. A. Marcus, *J. Chem. Phys*, **84**, 4894 (1986).
50. I. Rips and J. Jortner, *J. Chem. Phys.*, **87**, 2090 (1987).
51. D. H. Waldeck and D. E. Khoshtariya, *Applications of Electrochemistry and Nanotechnology in Biology and Medicine I* (Springer, New York, NY) 105 (2011).
52. H. Yue, D. Khoshtariya, D. H. Waldeck, J. Grochol, P. Hildebrandt, and D. H. Murgida, *J. Phys. Chem. B*, **110**, 19906 (2006).
53. S. Seyedi, M. M. Waskasi, and D. V. Matyushov, *J. Phys. Chem. B*, **121**, 4958 (2017).
54. S. Terrettaz, J. Cheng, and C. J. Miller, *J. Am. Chem. Soc.*, **118**, 7857 (1996).
55. A. M. Becka and C. J. Miller, *J. Phys. Chem.*, **96**, 2657 (1992).
56. D. R. Martin and D. V. Matyushov, *J. Chem. Phys. J. Chem. Phys.*, **142**, 161101 (2015).
57. A. M. Barragan, A. V. Soudackov, Z. Luthey-Schulten, S. Hammes-Schiffer, K. Schulten, and I. A. Solov'yov, *J. Am. Chem. Soc.*, **143**, 715 (2021).
58. D. R. Martin and D. V. Matyushov, *Sci. Rep.*, **7**, 5495 (2017).
59. S. M. Sarhangi and D. V. Matyushov, *J. Phys. Chem. B, in print* (2022).
60. D. R. Martin and D. V. Matyushov, *Phys. Chem. Chem. Phys.*, **17**, 22523 (2015).
61. M. M. Waskasi, D. R. Martin, and D. V. Matyushov, *J. Phys. Chem. B*, **122**, 10490 (2018).
62. D. W. Small, D. V. Matyushov, and G. A. Voth, *J. Am. Chem. Soc.*, **125**, 7470 (2003).
63. C. C. Moser, C. C. Page, and P. L. Dutton, *Phil. Trans. R. Soc. London B*, **361**, 1295 (2006).
64. S. Lindsay, *Life*, **10**, 72 (2020).